

Variability of Broad Emission Lines in High-Luminosity, High-Redshift Quasars

Sui Chi Woo¹ *, David A. Turnshek¹, Carles Badenes¹, and Steven Bickerton²

¹*PITTSburgh Partical physics, Astrophysics and Cosmology Center (PITT PACC), Department of Physics and Astronomy, University of Pittsburgh, Pittsburgh, PA 15260, USA*

²*Department of Astrophysical Sciences, Princeton University, Princeton NJ, USA*

ABSTRACT

We examine the variability of the high-ionization Ly α λ 1216 broad emission line (BEL) in a sample of 61 high-luminosity, high-redshift quasars observed at two epochs by the Sloan Digital Sky Survey. These bright objects lie in the redshift interval $z = [2.5, 4.3]$ and have luminosities $3.4 \times 10^{45} \lesssim \lambda L_\lambda \lesssim 3.4 \times 10^{46} \text{ erg s}^{-1}$ at 1450 Å. Utilizing improved spectrophotometric flux calibrations relative to nearby compact stars observed simultaneously, we are able to measure the flux changes in Ly α and the nearby continuum at two epochs. We find 20 objects that exhibit Ly α BEL flux variability at a significance level greater than 5σ on time-scales ranging from days to years in the quasar rest frame. The results show that, although some earlier work showed no significant detections of Ly α BEL flux changes in a quasar sample with even higher luminosity, variability is present and readily observable in the sample studied here. We also consider the CIV λ 1549 BEL. The lack of a strong correlation between Ly α BEL variability and nearby continuum variability is consistent with the presence of a time lag between the variations, whereas the presence of a stronger correlation between Ly α BEL variability and CIV BEL variability suggests that these BEL regions (BELRs) are at similar distances from the central ionizing source. Some interesting examples are high-lighted in the analysis, including a case where the flux of an Ly α BEL increased by $\sim 26\%$ in 14 days in the quasar rest frame, suggesting that the BELR has the shape of a disc, which is being observed face-on. This work demonstrates that future campaigns of spectrophotometric monitoring can improve our understanding of the structure of the BELRs of high-luminosity, high-redshift quasars.

Key words:

galaxies: active – galaxies: nuclei – galaxies: Seyfert – quasars: general

1 INTRODUCTION

Broad emission lines (BELs), such as Ly α , Nv and CIV, are prominent signatures seen in the optical/UV spectra of quasars. These lines arise in gas photoionized by the X-ray and UV continuum emission from the inner region of an accretion disc surrounding a supermassive black hole (SMBH) (Peterson 2011, 2006; Elvis 2010; Davis et al. 2007). Consequently, when continuum fluxes vary with time, BEL fluxes should respond to these variations but with time lags. Reverberation mapping studies of individual quasars and active galactic nuclei (AGN) can use results on time lags to determine the distances between central continuum sources and BEL regions (BELRs). Furthermore, these

size estimates for BELRs can be used with BEL velocity widths to infer the masses of SMBHs, under the assumption that the line-emitting regions are gravitationally bound to the SMBHs (Grier et al. 2012; Denney et al. 2010; Vestergaard & Peterson 2006; Kaspi et al. 2005). Deducing BELR size scales and SMBH masses are fundamental to understanding the physics of quasars.

There have been numerous reverberation mapping studies of lower luminosity, low-redshift AGN such as Seyfert galaxies. See, for example, Peterson (1993) and Peterson et al. (2004) for early reviews. Observationally such objects are brighter because they are nearby, and therefore variations are easier to detect. Also, their BELs tend to vary on shorter time-scales, of the order of light days to light weeks, and this permits more convenient temporal sampling to study the variability. Studies of lower lu-

* E-mail: suw11@pitt.edu

minosity AGN show that higher ionization BELs (e.g., Ly α and C IV) respond more rapidly to continuum variations than lower ionization BELs (e.g., H β , C III], and Mg II), indicating that lower ionization BELRs are farther out from the central source. In particular, the eight-month UV monitoring programme of NGC 5548 ($\lambda L_{\lambda} \sim 4.2 \times 10^{43}$ erg s $^{-1}$ at 1300 Å) found time lags of ~ 10 days for both Ly α and C IV, suggesting that these BELRs have similar size scales (Clavel et al. 1991).

To date, limited reverberation mapping work has been attempted on the more luminous quasars. Although quasars are known to be more energetic than AGN, they are usually significantly fainter than well-studied AGN due to their higher redshifts. Moreover, under the assumption that the photoionized BELRs of quasars and AGN have similar physical conditions, quasar BELR distances from the central source (and hence time lags) are expected to be larger by a factor of $\sim (L_{\text{quasar}}/L_{\text{AGN}})^{0.5}$, where L is luminosity. This is exacerbated by the fact that time lags in observed frames should be a factor of $1+z$ larger than in quasar/AGN rest frames due to cosmological considerations (i.e., at high redshifts we observe variations in “slow motion”). All of these effects make reverberation mapping studies of high-luminosity, high-redshift quasars more difficult and challenging.

While numerous studies have demonstrated that quasars have variable continua, few studies of their BEL variability have been made. O’Brien & Harries (1991) found a time lag of ~ 74 days between the UV continuum and the Ly α BEL in the luminous quasar 3C273. However, Ulrich et al. (1993) argued that the BEL variations were only marginally significant. A number of years ago Kaspi et al. (2007) reported no significant (i.e., $> 5\%$) Ly α BEL variability in a very luminous sample of high-redshift quasars.¹ However, they did report significant variations in the C IV BEL in response to continuum variations, leading to a time lag estimate of ~ 188 days in the quasar rest frame. Given these ambiguous results, it is not clear whether the Ly α BEL shows the same variability results as the C IV BEL, and whether reverberation mapping results from low-luminosity, low-redshift AGN can be scaled and applied to high-luminosity, high-redshift quasars.

Therefore, the goal of this paper is to investigate the variability of BELs in high-luminosity, high-redshift quasars. This would help clarify the feasibility of reverberation mapping studies for such a sample. To accomplish this we selected a sample from the Sloan Digital Sky Survey (SDSS) which had multiple spectral observations and we applied the spectrophotometric calibrations of Yip et al. (2009) to improve the spectrophotometry. In Section 2 we present the quasar sample, and we discuss the additional calibrations which can improve the relative spectrophotometric accuracy of the data. In Section 3 we outline how we measure flux changes in BELs and continua, and we present the results. Among other findings, our analyses show that $\sim 33\%$ of our sample exhibits significant ($> 5\sigma$) Ly α BEL flux variations.

¹ The sample studied here is not as luminous. The luminosities of our sample at 1450Å after galactic extinction corrections range from 3.40×10^{45} to 3.40×10^{46} erg s $^{-1}$, while their sample has luminosities from 2.76×10^{46} to 4.27×10^{47} erg s $^{-1}$.

These variations are not strongly correlated with nearby continuum variations, which is consistent with the presence of a time lag. However, a stronger statistical correlation between Ly α BEL flux variations and C IV BEL flux variations is seen, which suggests that these BELRs have similar size scales. In Section 4 we summarize the results and briefly discuss future prospects.

2 QUASAR DATA SET

2.1 Sample Definition

For this study we used the SDSS data release (DR8, Aihara et al. (2011)) to select an appropriate sample of quasars. In the observed frame SDSS spectra cover the optical to near-infrared (3800 – 9200 Å) with resolution $\lambda/\Delta\lambda \sim 2000$ at 5000 Å (Stoughton et al. 2002). To define our quasar sample and ensure that Ly α $\lambda 1216$ BELs are included in the spectra, we selected objects which are spectroscopically classified as QSOs, have redshifts in the interval $z = [2.5 - 5.0]$, and have multiple spectroscopic observations. The spectral classifications given in DR8 are highly reliable, with 98% accuracy in two independent reduction pipelines (spectro1d and idlspec2d). We excluded quasars observed using different plates on different dates to avoid possible calibration problems. Reasons for repeat spectroscopic observations in the SDSS are described in Wilhite et al. (2005). The repeat observations span time intervals ranging from days to years in the observed frame, leading to interesting durations for probing spectral variability in the quasar rest frames. In addition to the wide range of time intervals, the large sample size and homogeneity of SDSS spectroscopic data provide a unique advantage.

We found 407 quasars meeting the above criteria in DR8. Since variability in the observed frame at these higher redshifts is generally expected to increase with time interval, we have used only the first and last observations in order to maximize the time interval when more than two observations at different dates with the same plate exist.

2.2 Refinement of the Spectrophotometric Calibration

The work of Vanden Berk et al. (2004) and Wilhite et al. (2005) demonstrates that some additional spectrophotometric calibrations of SDSS spectra can be applied to increase the accuracy of spectral variability studies. Wilhite et al. (2005) used the stars to derive calibration differences between same-plate pairs, under the assumption that the majority of stars are non-variable. Later Yip et al. (2009) adopted a slightly different methodology, using galaxies instead of stars, since galaxies should be non-variable. Yip et al. (2009) estimated that their method improves the relative flux calibration between plate pairs by about a factor of two. The two-step calibration methods we used in this study are summarized below. See Yip et al. (2009) for a complete discussion.

First, to achieve an improved relative flux calibration for objects on a pair of plates taken at different modified Julian dates (MJDs), a wavelength-dependent flux ratio correction calibration is derived and applied. This is step one.

This is done by employing corrections made available by Yip et al. (2009). Their final corrections were derived from fifth-order polynomial least-squares fits, which provide low-order spectral corrections and eliminate higher-order spurious spectral features. These corrections were available for plate pairs in our sample up to DR6. Therefore, this further limited our sample size, since only 181 of the 407 plate pairs in our DR8 sample had an available wavelength-dependent calibration correction. This correction was applied to all 181 objects to search for variability.

Secondly, for significantly variable quasars, which are identified after step one and which require closer examination, we can derive and apply a wavelength-independent (i.e., grey) flux normalization correction using measurements of nearby non-variable compact objects surrounding a quasar.² This improves the relative spectrophotometric calibration between plates. We call this correction C_{band} , where “band” refers to the rest wavelength intervals specified below. Instead of choosing a narrow wavelength band at $6450 \text{ \AA} \pm 520 \text{ km s}^{-1}$ as suggested in Yip et al. (2009), we use the entire region from just longward of Ly α to longward of C IV, but exclude the locations of prominent emission lines. The rest frame wavelength bands which we use to derive C_{band} are 1260–1286, 1318–1380, 1430–1525, and 1580–1620 \AA .³ Table 1 gives examples of the additional improvements that can be achieved by presenting before and after C_{band} corrections for four selected quasars and nearby non-variable compact objects. These four example quasars are further discussed in Section 3.4. After C_{band} corrections are applied, compact objects should show no significant variability, and this turns out to be the case.

In summary, as outlined above, we implemented the first step to improve the wavelength-dependent spectrophotometric calibration and then the second step to improve the wavelength-independent relative spectrophotometric calibration, before we performed the variability analysis in Section 3.

2.3 Elimination of Problematic Objects

2.3.1 Poor Sky Subtraction

Sky subtraction of SDSS spectra is done in an automated data reduction pipeline. Wild & Hewett (2010) have pointed out that significant systematic residuals can remain in SDSS sky-subtracted spectra due to sub-optimal subtraction of the strong OH sky emission lines longward of 6700 \AA . In addition, we have found that some lower signal-to-noise ratio (S/N) spectra (e.g., spectra of fainter high-redshift quasars initially selected for this study) can suffer from poor sky

subtraction, leading to false-positive results on spectral variability. For the two observation epochs of our sample of 181 quasars, we plot in Figure 1 the average synthetic r-band magnitude derived from the SDSS spectra versus the average spectral S/N. As expected, S/N is seen to decrease with increasing magnitude. However, for average $r > 19.7$ or average S/N < 10 we have identified cases of false-positive results when performing our variability analysis. A clear indication of potential problems can be seen by examining data for the faint quasar SDSS J101840.46+285000.7, which has average $r \approx 22.3$ and average spectral S/N ≈ 0.9 . In our initial analysis of this object we detected significant flux variations over the entire range of observed wavelengths in just ~ 2.5 days in the quasar rest frame. However, examination of the sub-exposures (Bickerton et al. 2012), which were used to form the SDSS spectra at the two epochs, showed that poor sky subtraction was responsible for the apparent flux variations. The initial epoch spectrum was formed from nine sub-exposures and the final epoch spectrum was formed from three sub-exposures. Figure 2 illustrates the correlations between fluctuating sky spectra and Ly α + Nv BEL fluxes and nearby continuum fluxes (see Section 3.1 for how these were measured), respectively, over 12 sub-exposures.⁴ Following the initial analysis of our sample we have concluded that a reliable search for spectral variability requires the exclusion of objects with average r -band magnitudes fainter than ~ 19.7 and average spectral S/N < 10 . This reduces our sample to 64 quasars.

2.3.2 Discrepant Redshifts

When considering quasar redshift information for our sample we had to exclude three objects because the SDSS pipeline redshifts were discrepant: SDSS J101449.56+032600.8, SDSS J105905.06+272755.4, and SDSS J115852.86–004301.9.⁵ This reduces the size of our final sample to 61 quasars with luminosities $\lambda L_{\lambda} > 3.4 \times 10^{45} \text{ erg s}^{-1}$ at 1450 \AA and redshifts $z = [2.5, 4.3]$.

3 VARIABILITY ANALYSIS

Due to S/N differences and velocity offsets among different measured BELs, the SDSS pipeline usually calculates slightly different emission redshifts for the pair of spectra being analysed. Also, Wild & Hewett (2010) have shown that SDSS quasar redshifts possess systematic biases of $\sim 600 \text{ km s}^{-1}$. For consistency, and because of the effects mentioned above, we take two precautions when performing our analysis. First, we calculate a single redshift by averaging the pair of redshifts available for the two spectra. We then shift each spectrum into the rest frame of the quasar for subsequent analysis. The rest-frame wavelength region of interest

² A better approach might involve using galaxies to further improve the flux calibration, since they are clearly non-variable. However, because galaxies are extended and quasars are compact, possible variations in seeing between plate epochs make this approach problematic.

³ The derived C_{band} results for each compact object change less than a few percent when the wavelength intervals are reduced by a factor of two to 1260–1273, 1318–1349, 1430–1478, and 1580–1600 \AA . Thus, derived C_{band} corrections are robust and reasonably optimized.

⁴ Initially we considered the Ly α + Nv BEL blend, but later we focus on the Ly α BEL. For the analysis presented in Figure 2, we measured the Ly α + Nv BELs, but for the subsequent analyses we measured the Ly α BEL.

⁵ For SDSS J101449.56+032600.8 and SDSS J105905.06+272755.4, the BELs are incorrectly identified so the redshifts are incorrect. For SDSS J115852.86–004301.9, the classification of QSO is incorrect.

was chosen to be 1100–1700 Å so that the regions containing Ly α λ 1216 BELs and CIV λ 1549 BELs are included. Secondly, as discussed below, when measuring BEL fluxes, we use a velocity window which is large enough to ensure that typical velocity offsets will not significantly affect the results.

As discussed in the next two sections, we use two methods to make two different kinds of comparison to assess variability. Both methods rely on determining and subtracting the continua underneath the BELs in each spectrum. In the first method flux differences of BELs and continua between the two spectra are considered. In the second method, flux ratios of BELs and continua between the two spectra are considered.

3.1 Continuum and BEL Flux Changes

3.1.1 Continuum Changes

For each two-epoch pair of spectra we start by determining the mean continuum flux of each spectrum in the line-free regions near the Ly α BEL, defined as 1276–1286 Å and 1318–1334 Å, which ensures that the region in the vicinity of any OI λ 1302 BEL is excluded. Also, if necessary, any bad spectral regions within these wavelength intervals are identified by visual inspection and excluded. The spectrum with higher S/N in the observed r-band in the two-epoch pair is labeled HSN, whereas LSN refers to the one with lower S/N. The continuum flux difference at \sim 1300 Å is determined by subtracting the LSN-epoch mean flux from the HSN-epoch mean flux: $\Delta F_{c1300} = F_{c1300,HSN} - F_{c1300,LSN}$. The normalized flux change in the continuum is then defined to be $\Delta F_{c1300}/F_{c1300,HSN}$. Since the change in continuum level near \sim 1300 Å is as near as we can get to the ionizing continuum, we use this wavelength to measure the continuum change throughout this study. Standard deviations are determined by propagating the SDSS pipeline flux errors. Twenty-nine objects exhibit continuum flux changes at levels of significance $> 5\sigma$.

3.1.2 Ly α BEL Flux Changes

To study flux variations in the Ly α BEL we chose 1204–1229 Å as the region of interest (i.e., a region encompassing \approx 6170 km s $^{-1}$ around the BEL). This generally covers most of the flux in a Ly α BEL and is selected to mostly avoid inclusion of the nearby NV λ 1240 BEL. Thus, the chosen interval is a practical fixed choice not intended to match the observed width of the Ly α BEL, but it is suitable for the purpose of this study. The measured change in BEL flux can weakly depend on the chosen wavelength interval.⁶ To determine the continuum level to subtract underneath a Ly α BEL we use the mean continuum flux in the nearby continuum (Section 3.1.1). This works as well as an extrapolated straight-line fit. An extrapolated higher-order polynomial

⁶ Also, a flux change might vary across the BEL profile. For example, one or both of the BEL wings could show changes that are different than changes in the BEL core. We searched for clear indications of such behaviour by considering the central half of the original velocity interval (i.e., 1210–1223 Å), but found no clear examples of this. However, see Section 3.4.3.

fit would be inappropriate. Unfortunately, the region shortward of the Ly α BEL is generally depressed by the Ly α forest in the moderate resolution SDSS spectra, so this region could not be used to help determine the continuum level underneath the Ly α BEL. The absolute Ly α BEL fluxes in the HSN and LSN pair of spectra are then $F_{Ly\alpha,HSN}$ and $F_{Ly\alpha,LSN}$, respectively. Consistent with our previous definitions for a change in the continuum, the Ly α BEL flux difference is $\Delta F_{Ly\alpha} = F_{Ly\alpha,HSN} - F_{Ly\alpha,LSN}$ and the normalized Ly α BEL flux difference is $\Delta F_{Ly\alpha}/F_{Ly\alpha,HSN}$.

Figure 3 shows the distribution of normalized Ly α BEL flux changes versus normalized continuum flux changes for the 61 sample quasars. Again, the standard deviations shown for the plotted points are determined by propagating the SDSS pipeline flux errors. Twenty quasars (shown in red) show Ly α BEL flux variations at a significance level $> 5\sigma$. Among these 20 quasars we have selected four to discuss in Section 3.4.

As an illustration of what the results shown in Figure 3 might mean we have parametrized how flux changes in a hypothetical, but typical, Ly α BEL profile and the associated nearby continuum would appear in this plot. To do this we parametrize a continuum-normalized HSN spectrum as

$$f_{HSN}(\lambda) = 1 + Ae^{-\left(\frac{\lambda-1216\text{\AA}}{\delta\lambda}\right)^2}, \quad (1)$$

where A is the amplitude of the Ly α BEL peak at 1216 Å relative to the normalized continuum and $\delta\lambda$ sets the line width. For this illustration we put $A = 5.5$ and $\delta\lambda = 12$ Å (\sim 3000 km s $^{-1}$), which are typical. The hypothetical LSN spectrum is then parametrized as

$$f_{LSN}(\lambda) = a_1 + a_2 Ae^{-\left(\frac{\lambda-1216\text{\AA}}{\delta\lambda}\right)^2}, \quad (2)$$

where a_1 and a_2 dictate how the flux in the continuum and Ly α BEL change, respectively. A grid of a_1 (on the dashed horizontal axis) and a_2 (on the dotted vertical axis) parameters are overplotted on Figure 3 to give an indication of the nature of the observed flux changes in our sample.

3.1.3 CIV BEL Flux Changes

Following the procedure we used to measure Ly α BELs in Section 3.1.2, we have also measured CIV BELs. However, the continuum levels we subtract from CIV BELs are measured at 1470–1488 Å and 1600–1616 Å in the quasar rest-frames. We then measure the CIV BEL over the rest-frame interval 1534–1566 Å, which corresponds to a velocity interval that is similar to the one used for the Ly α BEL. Eight objects exhibit (shown in blue) CIV BEL flux changes at levels of significance $> 5\sigma$. In the bottom panel of Figure 3 we show $\Delta F_{CIV}/F_{CIV,HSN}$ versus $\Delta F_{c1300}/F_{c1300,HSN}$. On this bottom panel we also show the same grid of a_1 and a_2 values shown in the top panel of Figure 3 for the Ly α BELs. This permits a comparison between changes in the Ly α and CIV BELs.

3.1.4 Correlations between Flux Changes in the Continuum, Ly α BEL, and CIV BEL

Past monitoring campaigns of low-luminosity Seyfert 1s conducted with the *International Ultraviolet Explorer*

have revealed similar time lags for Ly α and CIV BELs (Korista et al. 1995). To check if this holds in our quasar sample, in Figure 4 we plot the normalized Ly α BEL flux changes versus the normalized CIV BEL flux changes. Analysis of the results shown in Figures 3 and 4 reveal correlations between the flux change results. After taking into account the variances of the data points, the correlation coefficients are: 0.43 for Ly α BEL flux changes versus continuum changes (Figure 3, top panel), 0.51 for CIV BEL flux changes versus continuum changes (Figure 3, bottom panel), and 0.74 for Ly α BEL flux changes versus CIV BEL flux changes (Figure 4). Thus, there is a significantly stronger correlation between observed changes in the two BELs, in comparison to correlations between changes in either BEL and the continuum.

3.2 Flux Ratios between the HSN and LSN Epochs

The second method we use to evaluate variability involves examining the ratio of spectral components at the two different epochs. This is useful because it provides a different way to assess our results. To evaluate this we consider $R_{\text{Ly}\alpha} = F_{\text{Ly}\alpha, \text{HSN}}/F_{\text{Ly}\alpha, \text{LSN}}$ versus $R_{c1300} = F_{c1300, \text{HSN}}/F_{c1300, \text{LSN}}$ and $R_{\text{CIV}} = F_{\text{CIV}, \text{HSN}}/F_{\text{CIV}, \text{LSN}}$ versus R_{c1300} in Figure 5 (top panel and middle panel, respectively). We also plot $R_{\text{Ly}\alpha}$ versus R_{CIV} in Figure 5 (bottom panel). The data shown in red in these figures are the same data originally plotted in red in Figures 3 and 4, i.e., objects showing absolute flux variations in the Ly α BEL at a level of significance $> 5\sigma$. Of course, when R values are unity it represents no flux change and when, for example, $R_{\text{Ly}\alpha} = R_{c1300}$ it indicates that the Ly α BEL and the nearby continuum experienced the same fractional increase or decrease in flux (i.e., grey scaling). The results generally confirm the findings of Section 3.1.4. After taking into account the variances of the flux ratios, the correlation coefficients are: 0.54 for $R_{\text{Ly}\alpha}$ versus R_{c1300} (Figure 5, top panel), 0.69 for R_{CIV} versus R_{c1300} (Figure 5, middle panel), and 0.76 for $R_{\text{Ly}\alpha}$ versus R_{CIV} (Figure 5, bottom panel).

3.3 Time Variations

For our sample of 61 high-luminosity, high-redshift quasars, the top, middle and bottom panels of Figure 6 show results on the fractional changes in Ly α BEL flux, CIV BEL flux and continuum flux, respectively, as a function of time between observation epochs in the quasar rest frame, $\Delta\tau$.

3.4 Examples of Detected Variations

From the 20 quasars with $> 5\sigma$ Ly α BEL variations shown in Figure 3 (red points), we select four representative cases to illustrate. Table 2 summarizes the two-epoch flux measurements of the BELs and continua for these four quasars, along with their associated emission redshifts, rest-frame time interval $\Delta\tau$ between the two observation epochs, r-band magnitudes, and Galactic extinction-corrected (Schlafly & Finkbeiner 2011) luminosities at rest-frame 1450Å. This information for all 61 quasars can be

found in an expanded version of Table 2, which is available in the electronic version of the journal.

The spectral changes in the four quasars are shown in Figures 7–10. The red and blue curves in the figures represent the spectra at HSN epochs and LSN epochs, respectively. The overplotted black solid lines are the spline fits to the continua and BELs. The dark red curve in the top panel of the figures is the flux difference between the two epochs, whereas the dark red curve in the bottom panel is the flux ratio between the two epochs. A brief discussion of the four examples follows.

3.4.1 SDSS J004240.65+141529.6

The spectra of SDSS J004240.65+141529.6 ($z \approx 3.70$) are shown in Figure 7, ~ 14 days apart in the quasar rest frame. The redshift of the Ly α BEL is somewhat larger than indicated by the SDSS pipeline redshift, but the redshift of the CIV BEL is a close match. The measured Ly α BEL flux seen in the second LSN-epoch spectrum is $\sim 26\%$ fainter than in the first HSN-epoch spectrum, whereas the nearby continuum flux decreases only $\sim 6\%$. The relatively fast change in Ly α BEL flux in this quasar might be considered surprising given its high luminosity. For example, if the luminosity of this quasar is compared to the luminosity of AGN NGC 5548, we find: $(L_{\text{quasar}}/L_{\text{AGN}})^{0.5} \sim 13.6$. Of course, time lags can not be derived from two-epoch data. However, if BELRs are larger in luminous quasars, one might naively expect fractional Ly α BEL flux variations to be slower in high-luminosity objects. Yet the fractional variations seen in this quasar are comparable to the ones seen in NGC 5548 (Peterson 1994). The observed fast change suggests that a significant fraction of the Ly α BELR has a correspondingly small size scale along our sightline. For example, this would occur if the Ly α BELR were confined to a disc-like region, and we were viewing the disc close to face-on. In such a geometry the light travel time across the BELR along our sightline would be $\sim \sin(i)D_{\text{Ly}\alpha \text{ BELR}}$, where i is the inclination angle relative to the disc's polar axis and $D_{\text{Ly}\alpha \text{ BELR}}$ is the diameter of the Ly α BELR disc. Thus, this observation would support the idea that the Ly α BELR is due to disc emission. Alternatively, these short time-scale variations might indicate anisotropic emission from the BELR, as has been discussed by Perez et al. (1989).

3.4.2 SDSS J132750.44+001156.8

SDSS J132750.44+001156.8 (Figure 8, $z = 2.53$) shows increases in the Ly α BEL flux and nearby continuum flux of ~ 34 and ~ 12 per cent during a period of ~ 84 days in the quasar rest frame. The BELs are very broad, such that the wings of the Ly α and CIV BELs are not included in the $\sim 6200 \text{ km s}^{-1}$ interval that we measure. Relative to the SDSS pipeline redshift, the redshift of the peak of the Ly α BEL appears higher and the redshift of the peak of the CIV BEL appears lower. A significant flux change in the CIV BEL is not observed. The continuum spectral slope at the brighter HSN-epoch is bluer than observed at the LSN-epoch.

3.4.3 SDSS J095106.32+541149.8

The spectra of SDSS J095106.32+541149.8 (Figure 9, $z = 2.69$) were taken ~ 610 days apart in the quasar rest frame. Significant flux changes in both the Ly α and C IV BELs are present, whereas no significant change in the nearby continuum flux is observed. Relative to the initial LSN-spectrum the Ly α BEL flux increased $\sim 25\%$, the nearby continuum flux increased $\sim 1\%$, and the C IV BEL flux increased $\sim 20\%$. The redshift of the Ly α BEL is consistent with the SDSS redshift, but the redshift of the C IV BEL is somewhat lower. The Ly α BEL may show a larger flux change in the line core than in the wing.

3.4.4 SDSS J120802.64+630328.9

The spectra of SDSS J120802.64+630328.9 (Figure 10, $z = 2.57$) were taken ~ 613 days apart in the quasar rest frame. No significant flux changes in both the Ly α and C IV BELs are observed, whereas a significant change in the nearby continuum flux is present. Relative to the initial HSN-spectrum the Ly α BEL flux increased $\sim 2\%$, the nearby continuum flux increased $\sim 23\%$, and the C IV BEL flux decreased $\sim 7\%$. The redshift of the Ly α BEL is consistent with the SDSS redshift, but the redshift of the C IV and N V BEL is somewhat lower. A strong damped Ly α (DLA) absorption-line system, which is intervening and unrelated to the quasar, is identified at a redshift of $z_{abs} = 2.442$.

3.5 Correlations and their Dependence on Time Interval and Luminosity

In order to study any correlations that may depend on the time interval between observations and the quasar luminosity, we have formed a new parameter $\Delta\tau' = \Delta\tau / (L_{quasar}/L_{AGN})^{0.5}$. If the variation time increases in proportion to $(L_{quasar}/L_{AGN})^{0.5}$, $\Delta\tau'$ would scale the time intervals to take such an effect into account. We have used $L_{AGN} = 4.2 \times 10^{43}$ ergs s^{-1} , which is the luminosity of NGC 5548 at 1300 Å. We then divide our sample in half according to $\Delta\tau'$. Half of our sample has $\Delta\tau' < 1.35$ days and half has $\Delta\tau' > 1.35$ days. Since we found that changes in the Ly α and C IV BELs are well correlated, we have also averaged the individual change results on Ly α and C IV to form a variance-weighted average ΔF_{BEL} . The correlation between BEL flux changes versus continuum changes is then considered for our sample for short ($\Delta\tau' < 1.35$ days) and long ($\Delta\tau' > 1.35$ days) luminosity-scaled, rest-frame time intervals. The results are shown in Figure 11. We find that there is a strong correlation between BEL flux change and continuum change when $\Delta\tau' < 1.35$ days (correlation coefficient of 0.74), but the correlation is much weaker when $\Delta\tau' > 1.35$ days (correlation coefficient of 0.29). Thus, the overall trend seen in our sample is for BEL and continuum variations to become less correlated for the longer luminosity-scaled, rest-frame time intervals. We found this interesting, but the origin of this effect is unclear.

4 SUMMARY AND DISCUSSION

We have investigated the variability of the Ly α BEL in a sample of 61 quasars observed at two epochs by the SDSS. The quasars have redshifts that lie in the interval $z = [2.5, 4.3]$ and luminosities $3.4 \times 10^{45} \lesssim \lambda L_{\lambda} \lesssim 3.4 \times 10^{46}$ ergs s^{-1} at 1450 Å. Variability of the Ly α BEL is ubiquitous in our sample on rest-frame time-scales ranging from days to years, with ~ 33 per cent of the sample showing Ly α BEL variations $> 5\sigma$. Thus, despite some earlier work which reported no significant Ly α BEL flux variations in a somewhat higher luminosity sample than ours, variability is clearly present and readily observable in the luminous sample of high-redshift quasars studied here.

However, during the work that led us to consider our final sample of 61 quasars, examination of the SDSS sub-exposures led us to conclude that faint ($r > 19.7$ mag) and low S/N (< 10) spectra may produce unreliable results.

In addition to measuring variations in the Ly α BEL, we also measured the corresponding continuum and C IV BEL variations. Even with two-epoch data, some interesting trends are seen in our sample. For example, there is not a strong correlation between Ly α BEL variability and nearby continuum variability, and this is consistent with the presence of a time lag between the variations. However, there is a strong correlation between Ly α BEL variability and C IV BEL variability, and this suggests that these BELRs are at similar distances from the central ionizing source.

Finally, some interesting examples are emphasized in the analysis. For example, in one case (SDSS J004240.65+141529.6) the flux of an Ly α BEL increased by ~ 26 per cent in only 14 days in the quasar rest frame. This probably indicates that a significant fraction of the Ly α BELR has a correspondingly small size scale along our sightline. In the absence of anisotropic Ly α emission from the BELR, the most likely reason for this fast change would be that the Ly α BELR has the shape of a disc, and we are viewing the disc close to face-on (Section 3.4.1). In such a geometry the light travel time across the BELR along our sightline would be $\sim \sin(i) D_{Ly\alpha\ BELR}$, where i is the inclination angle relative to the disc's polar axis and $D_{Ly\alpha\ BELR}$ is the diameter of the Ly α BELR disc. Thus, for example, this observation appears to be consistent with models where the BELR primarily originates in the chromosphere of a quasar's face-on accretion disc (Murray et al. 1995; Murray & Chiang 1997). If this is the case, such observations may some day provide constraints on quasar inclination angles, or at least allow us to identify quasars that have nearly face-on accretion discs. In any case, this work demonstrates that future campaigns of spectrophotometric monitoring can improve our understanding of the structure of the BELRs of high-luminosity, high-redshift quasars.

5 ACKNOWLEDGEMENT

We thank Ching-Wa Yip for providing the wavelength-dependent flux ratio corrections for our sample and all private discussions and Daniel Vanden Berk for some early discussions about variability analysis. We also acknowledge the referee for careful reading and useful comments.

Funding for the SDSS and SDSS-II has been provided

by the Alfred P. Sloan Foundation, the Participating Institutions, the National Science Foundation, the U.S. Department of Energy, the National Aeronautics and Space Administration, the Japanese Monbukagakusho, the Max Planck Society, and the Higher Education Funding Council for England. The SDSS website is <http://www.sdss.org/>.

The SDSS is managed by the Astrophysical Research Consortium for the Participating Institutions. The Participating Institutions are the American Museum of Natural History, Astrophysical Institute Potsdam, University of Basel, University of Cambridge, Case Western Reserve University, University of Chicago, Drexel University, Fermilab, the Institute for Advanced Study, the Japan Participation Group, Johns Hopkins University, the Joint Institute for Nuclear Astrophysics, the Kavli Institute for Particle Astrophysics and Cosmology, the Korean Scientist Group, the Chinese Academy of Sciences (LAMOST), Los Alamos National Laboratory, the Max-Planck-Institute for Astronomy (MPIA), the Max-Planck-Institute for Astrophysics (MPA), New Mexico State University, Ohio State University, University of Pittsburgh, University of Portsmouth, Princeton University, the United States Naval Observatory, and the University of Washington.

This research has made use of the NASA/IPAC Extragalactic Database (NED) which is operated by the Jet Propulsion Laboratory, California Institute of Technology, under contract with the National Aeronautics and Space Administration.

REFERENCES

- Aihara H., Allende Prieto C., An D., et al. 2011, *ApJS*, 193, 29
- Bickerton S., Badenes C., Hetteringer T., Beers T., Huang S., 2012, in Griffin E., Hanisch R., Seaman, R., eds., *IAU Symposium Vol. 285 of IAU Symposium, Time-Resolved Spectroscopy with SDSS*. pp 289–290
- Clavel J., Reichert G. A., Alloin D., Crenshaw D. M., Kriss G., Krolik J. H., Malkan M. A., Netzer H., Peterson B. M., Wamsteker W., Altamore A., Baribaud T., Barr P., Beck S., Binette L., 1991, *ApJ*, 366, 64
- Davis S. W., Woo J., Blaes O. M., 2007, *ApJ*, 668, 682
- Denney K. D., Peterson B. M., Pogge R. W., et al. 2010, *ApJ*, 721, 715
- Elvis M., 2010, in Peterson B. M., Somerville R. S., Storchi-Bergmann, T., eds., *IAU Symposium Vol. 267 of IAU Symposium, The Quasar Continuum*. pp 55–64
- Grier C. J., Peterson B. M., Pogge R. W., et al. 2012, *ApJ*, 744, L4
- Kaspi S., Brandt W. N., Maoz D., Netzer H., Schneider D. P., Shemmer O., 2007, *ApJ*, 659, 997
- Kaspi S., Maoz D., Netzer H., Peterson B. M., Vestergaard M., Jannuzi B. T., 2005, *ApJ*, 629, 61
- Korista K. T., Alloin D., Barr P., et al. 1995, *ApJS*, 97, 285
- Murray N., Chiang J., 1997, *ApJ*, 474, 91
- Murray N., Chiang J., Grossman S. A., Voit G. M., 1995, *ApJ*, 451, 498
- O’Brien P. T., Harries T. J., 1991, *MNRAS*, 250, 133
- Perez E., Penston M. V., Moles M., 1989, *MNRAS*, 239, 55
- Peterson B. M., 1993, *PASP*, 105, 247
- Peterson B. M., 1994, in Gondhalekar P. M., Horne K., Peterson B. M., eds., *Reverberation Mapping of the Broad-Line Region in Active Galactic Nuclei Vol. 69 of Astronomical Society of the Pacific Conference Series, Overview of Reverberation Mapping: Progress and Problems*. p. 1
- Peterson B. M., 2006, in D. Alloin, ed., *Physics of Active Galactic Nuclei at all Scales Vol. 693 of Lecture Notes in Physics*, Berlin Springer Verlag, *The Broad-Line Region in Active Galactic Nuclei*, P.77
- Peterson B. M., 2011, in L. Foschini, et al., eds., *Narrow-Line Seyfert 1 Galaxies and their Place in the Universe Masses of Black Holes in Active Galactic Nuclei: Implications for Narrow-Line Seyfert 1 Galaxies*, *Proceedings of Science (PoS, Trieste, Italy)*, vol. NLS1, Published online at <http://pos.sissa.it/cgi-bin/reader/conf.cgi?confid=126>, id.32
- Peterson B. M., Ferrarese L., Gilbert K. M., Kaspi S., Malkan M. A., Maoz D., Merritt D., Netzer H., Onken C. A., Pogge R. W., Vestergaard M., Wandel A., 2004, *ApJ*, 613, 682
- Schlafly E. F., Finkbeiner, D. P. 2011, *ApJ*, 737, 103
- Stoughton C., Lupton R. H., Bernardi M., et al. 2002, *AJ*, 123, 485
- Ulrich M.-H., Courvoisier T. J.-L., Wamsteker W., 1993, *ApJ*, 411, 125
- Vanden Berk D. E., Wilhite B. C., Kron R. G., Anderson S. F., Brunner R. J., Hall P. B., Ivezić Ž., Richards G. T., Schneider D. P., York D. G., Brinkmann J. V., Lamb D. Q., Nichol R. C., Schlegel D. J., 2004, *ApJ*, 601, 692
- Vestergaard M., Peterson B. M., 2006, *ApJ*, 641, 689
- Wild V., Hewett P. C., arXiv:1010.2500
- Wilhite B. C., Vanden Berk D. E., Kron R. G., Schneider D. P., Pereyra N., Brunner R. J., Richards G. T., Brinkmann J. V., 2005, *ApJ*, 633, 638
- Yip C. W., Connolly A. J., Vanden Berk D. E., Scranton R., Krughoff S., Szalay A. S., Dobos L., Tremonti C., Taghizadeh-Popp M., Budavári T., Csabai I., Wyse R. F. G., Ivezić Ž., 2009, *AJ*, 137, 5120

Table 1. Flux ratios for four quasars and surrounding compact objects before and after the grey recalibration correction.

Quasars			Compact Objects			
SDSS J	$C_{\text{band}}^{\text{before}}$ ¹	SDSS J	$C_{\text{band}}^{\text{before}}$ ¹	$\overline{C}_{\text{band}}^{\text{before}}$ ²	$\overline{C}_{\text{band}}^{\text{after}}$ ³	
1	004240.65+141529.6	003408.61+134839.0	0.986	0.984±0.015	1.000±0.015	
		003448.91+134439.3	0.955			
		003441.35+153517.8	1.055			
		003651.49+145035.9	0.986			
		003854.02+143742.9	0.969			
		003707.21+155552.5	0.951			
2	132750.44+001156.8	132456.66−010534.6	1.185	1.177±0.012	1.000±0.010	
		132304.59+000924.5	1.119			
		132634.99−011108.2	1.127			
		132730.91−011024.8	1.218			
		132404.47−004428.8	1.179			
		132510.57−003233.6	1.202			
		133136.77+001959.3	1.206			
3	095106.32+541149.8	094420.28+540810.2	1.193	1.172±0.029	1.000±0.025	
		094659.80+544546.7	1.191			
		094920.08+543803.2	1.030			
		095003.13+541821.7	1.217			
		095253.45+550957.7	1.231			
4	120802.64+630328.9	115510.14+624653.5	1.048	1.047±0.002	1.000±0.002	
		120039.52+623428.5	1.113			
		121642.58+623405.9	0.978			
		121425.49+623009.0	1.050			

Note. — We use the rest-frame wavelength bands at 1260–1285 Å, 1318–1380 Å, 1430–1525 Å and 1580–1620 Å, ensuring no prominent emission lines at the chosen regions in four quasars.

¹Flux ratio $C_{\text{band}}^{\text{before}}$ of each object before recalibration using the method of Yip et al. (2009).

²Mean of $C_{\text{band}}^{\text{before}}$ of the compact objects in each group before recalibration using the method of Yip et al. (2009).

³Mean of $C_{\text{band}}^{\text{after}}$ of the compact objects in each group after applying the recalibration.

Table 2. BEL and continuum flux measurements for four quasars after recalibration using surrounding compact objects

	MJD				$\Delta\tau$		$\lambda L_{1450\text{\AA}}$ (ergs s^{-1})	HSN-epoch				LSN-epoch			
	SDSS J (1)	HSN (2)	LSN (3)	z_{em} (4)	(days) (5)	r (6)		$F_{Ly\alpha}$ (8)	$F_{c1300\text{\AA}}$ (9)	F_{CIV} (10)	$F_{c1600\text{\AA}}$ (11)	$F_{Ly\alpha}$ (12)	$F_{c1300\text{\AA}}$ (13)	F_{CIV} (14)	$F_{c1600\text{\AA}}$ (15)
1	004240.65+141529.6	51817	51884	3.70	14.08	19.20	9.31×10^{45}	6.15 ± 0.11	4.55 ± 0.05	1.77 ± 0.08	3.87 ± 0.06	4.52 ± 0.10	4.28 ± 0.06	1.49 ± 0.07	3.78 ± 0.05
2	132750.44+001156.8	51959	51663	2.53	83.88	18.44	1.03×10^{46}	9.93 ± 0.23	17.56 ± 0.14	0.83 ± 0.15	13.93 ± 0.10	7.43 ± 0.23	15.55 ± 0.15	0.84 ± 0.16	13.20 ± 0.11
3	095106.32+541149.8	54530	52282	2.69	609.65	18.89	8.45×10^{45}	23.28 ± 0.18	12.45 ± 0.09	6.29 ± 0.11	9.71 ± 0.08	18.69 ± 0.21	12.37 ± 0.12	5.26 ± 0.16	9.93 ± 0.11
4	120802.64+630328.9	52337	54525	2.57	612.65	17.70	3.30×10^{45}	46.93 ± 0.31	48.48 ± 0.17	16.59 ± 0.22	36.96 ± 0.12	47.78 ± 0.37	59.65 ± 0.20	17.68 ± 0.24	43.64 ± 0.15

Note. — All flux units are in $10^{-17} \text{ erg s}^{-1} \text{ cm}^{-2} \text{ \AA}^{-1}$. This information for all 61 quasars can be found in an expanded version of Table 2, which is available in the electronic version of the journal.

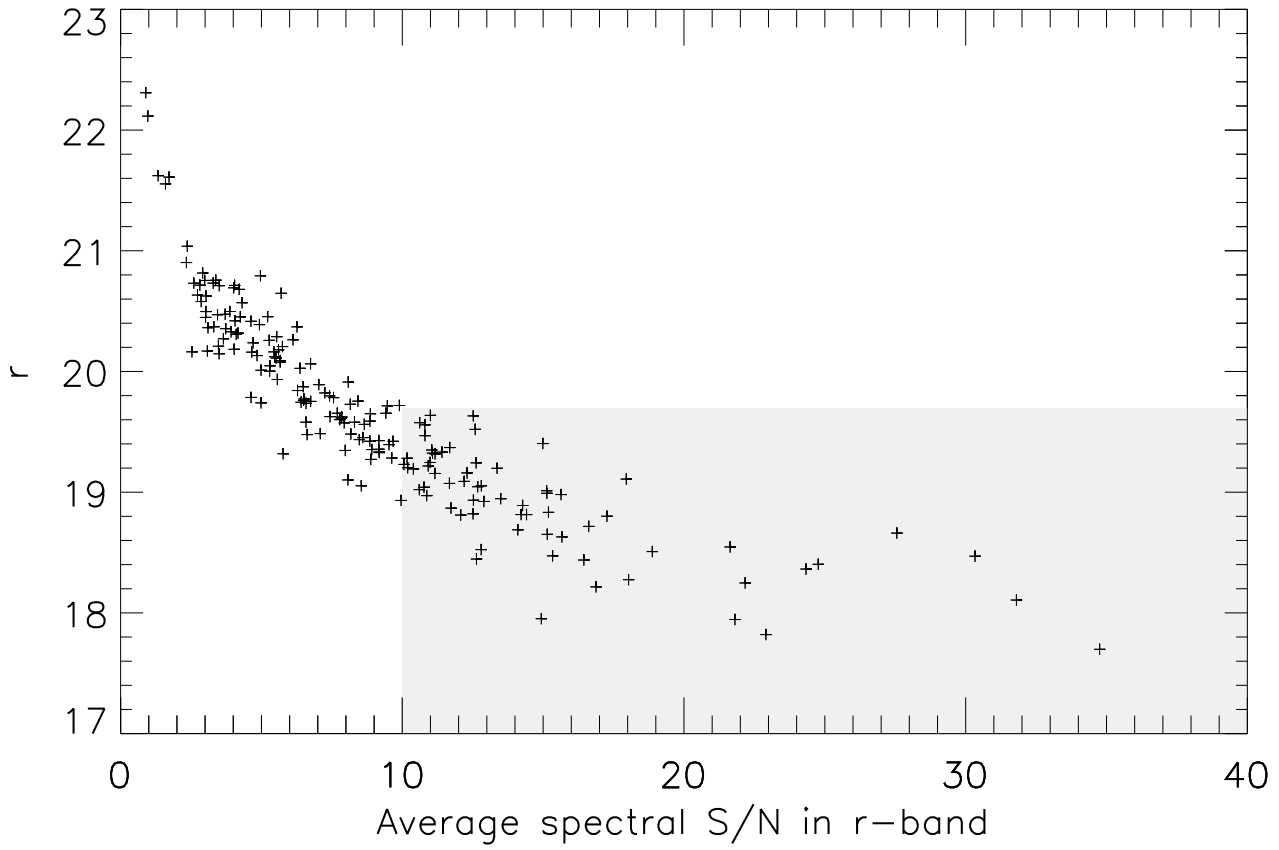


Figure 1. Average SDSS r -band magnitude measured from the spectra at two epochs versus average spectral S/N. Objects with S/N < 10 and r fainter than ~ 19.7 mag are eliminated from the final sample to avoid possible false-positive results on variability due to sky subtraction residuals.

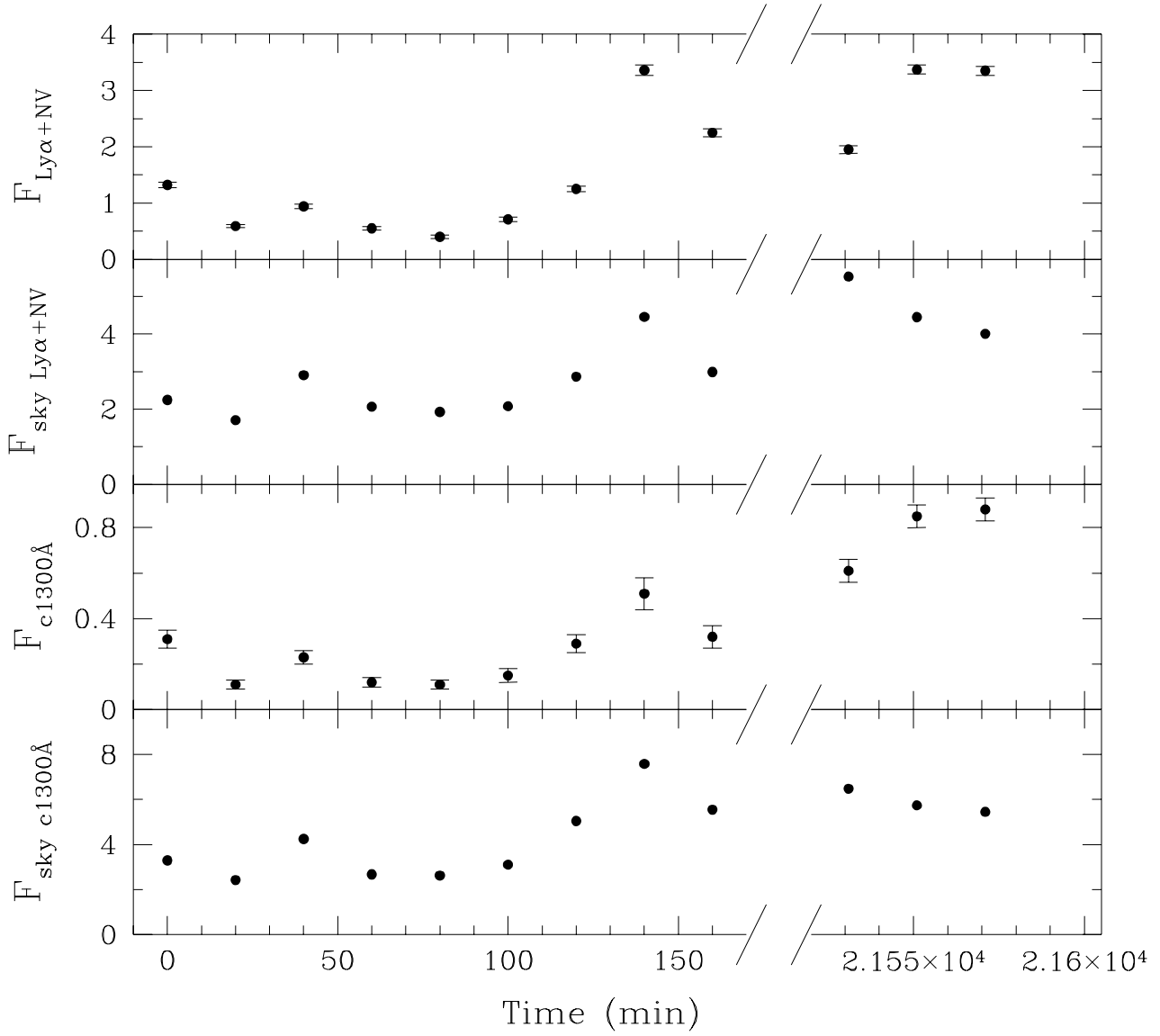


Figure 2. Faint quasar SDSS J101840.46+285000.7 with flux variations correlated to sky fluctuations in Ly α + NV BEL regions (top two) and nearby continuum regions (bottom two), respectively, over 12 sub-exposures. The unit of flux is $10^{-17} \text{ erg s}^{-1} \text{ cm}^{-2} \text{ \AA}^{-1}$.

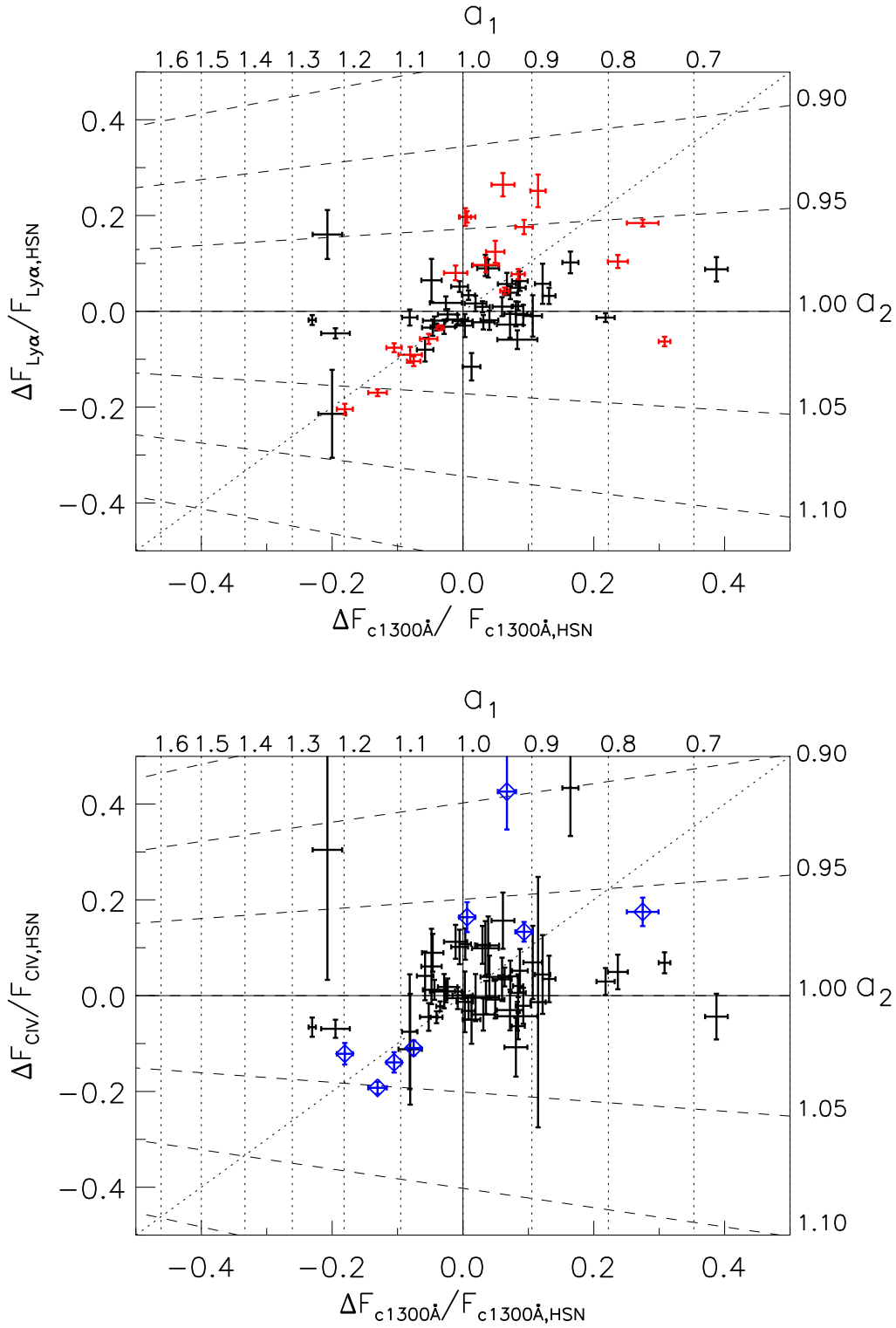


Figure 3. Top: The distribution of normalized Ly α BEL flux changes vs. normalized continuum flux changes for 61 quasars. Twenty quasars (red points) exhibit Ly α BEL flux variations at a significance level $> 5\sigma$. Bottom: The distribution of normalized CIV BEL flux changes vs. normalized continuum flux changes for 61 quasars. Eight quasars (blue diamonds) exhibit CIV BEL flux variations at a significance level $> 5\sigma$. We have parameterized flux changes in a hypothetical Ly α BEL profile and the associated nearby continuum in the parameter space of a_1 and a_2 . See the details in the text.

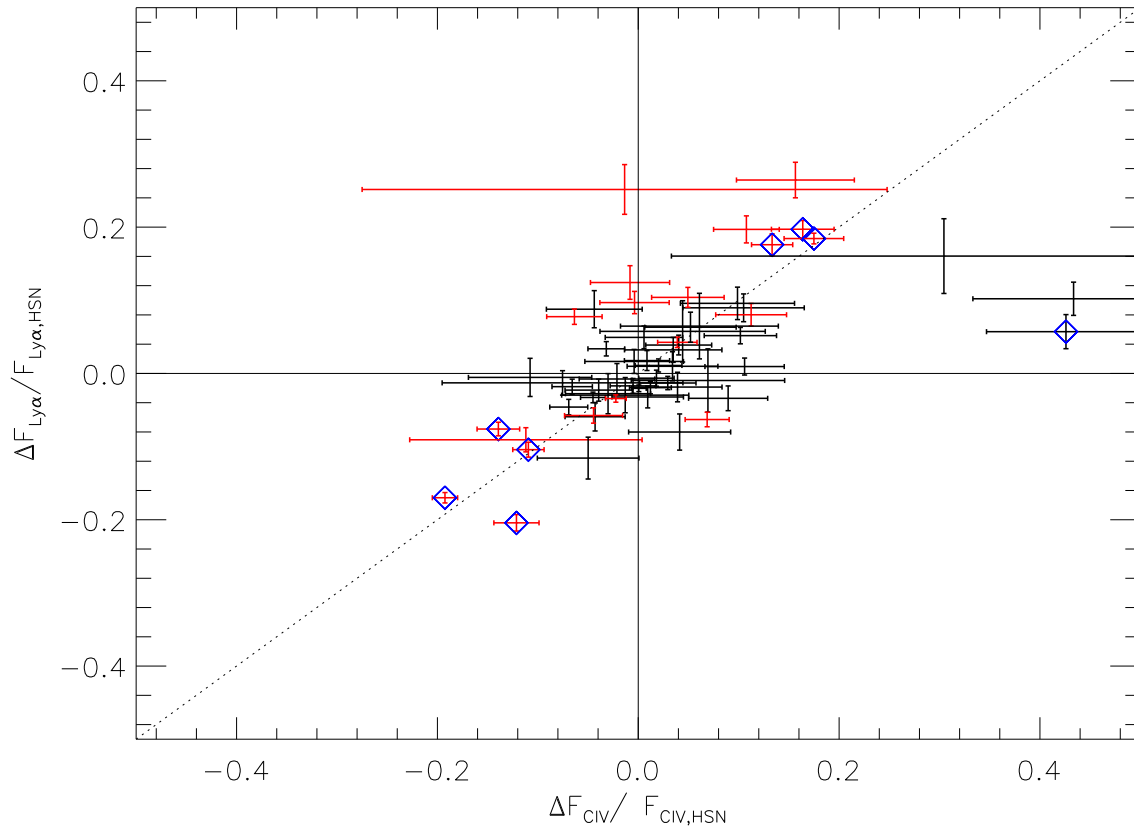


Figure 4. Fractional change in Ly α BEL flux vs. fractional change in CIV BEL flux between two epochs.

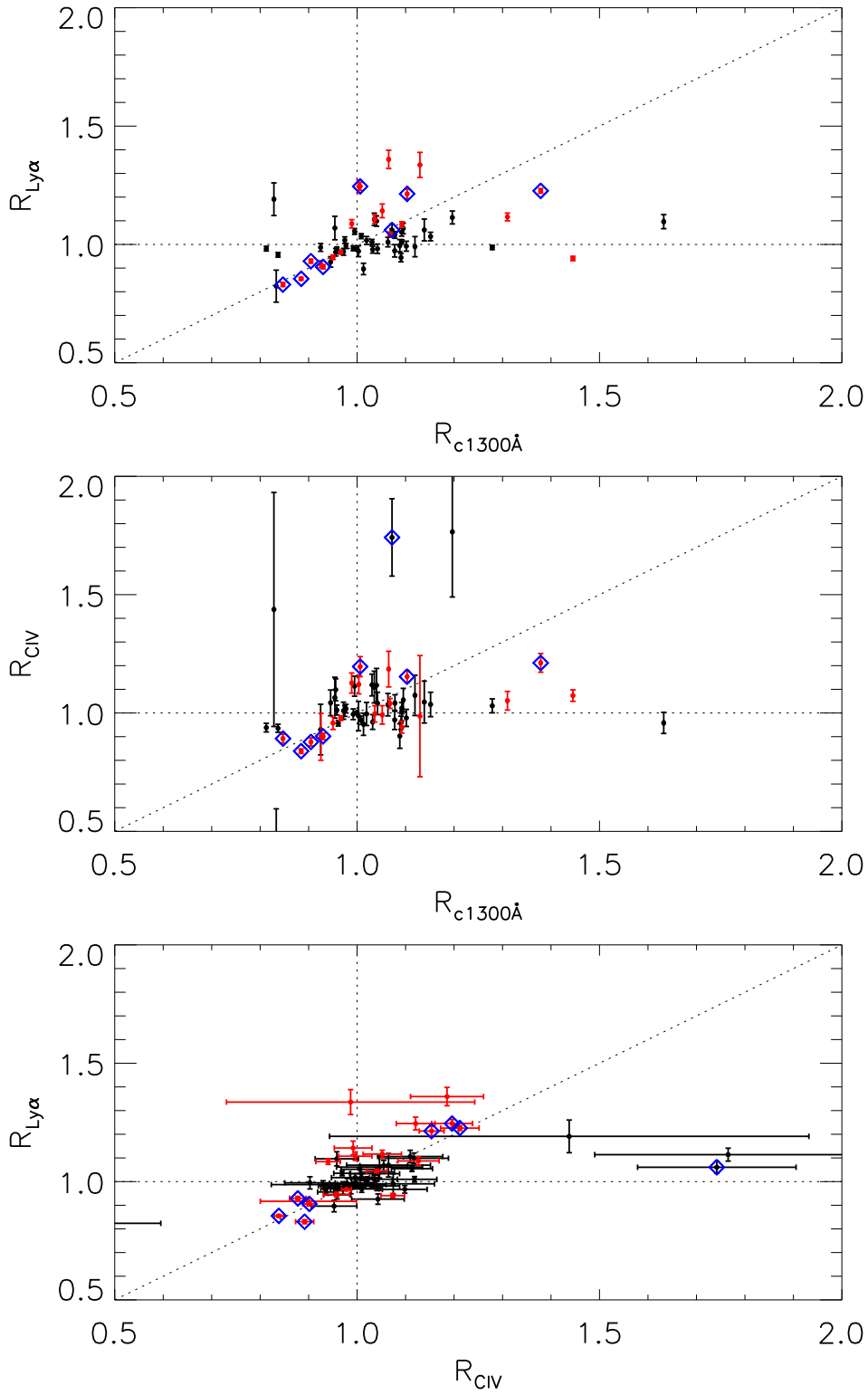


Figure 5. Top: Ly α BEL flux ratio vs. continuum flux ratio. Middle: CIV BEL flux ratio vs. continuum flux ratio. Bottom: Ly α BEL flux ratio vs. CIV BEL flux ratio. As in Figures 3 and 4, the red points and blue diamonds are those with Ly α and CIV BEL flux changes $> 5\sigma$, respectively.

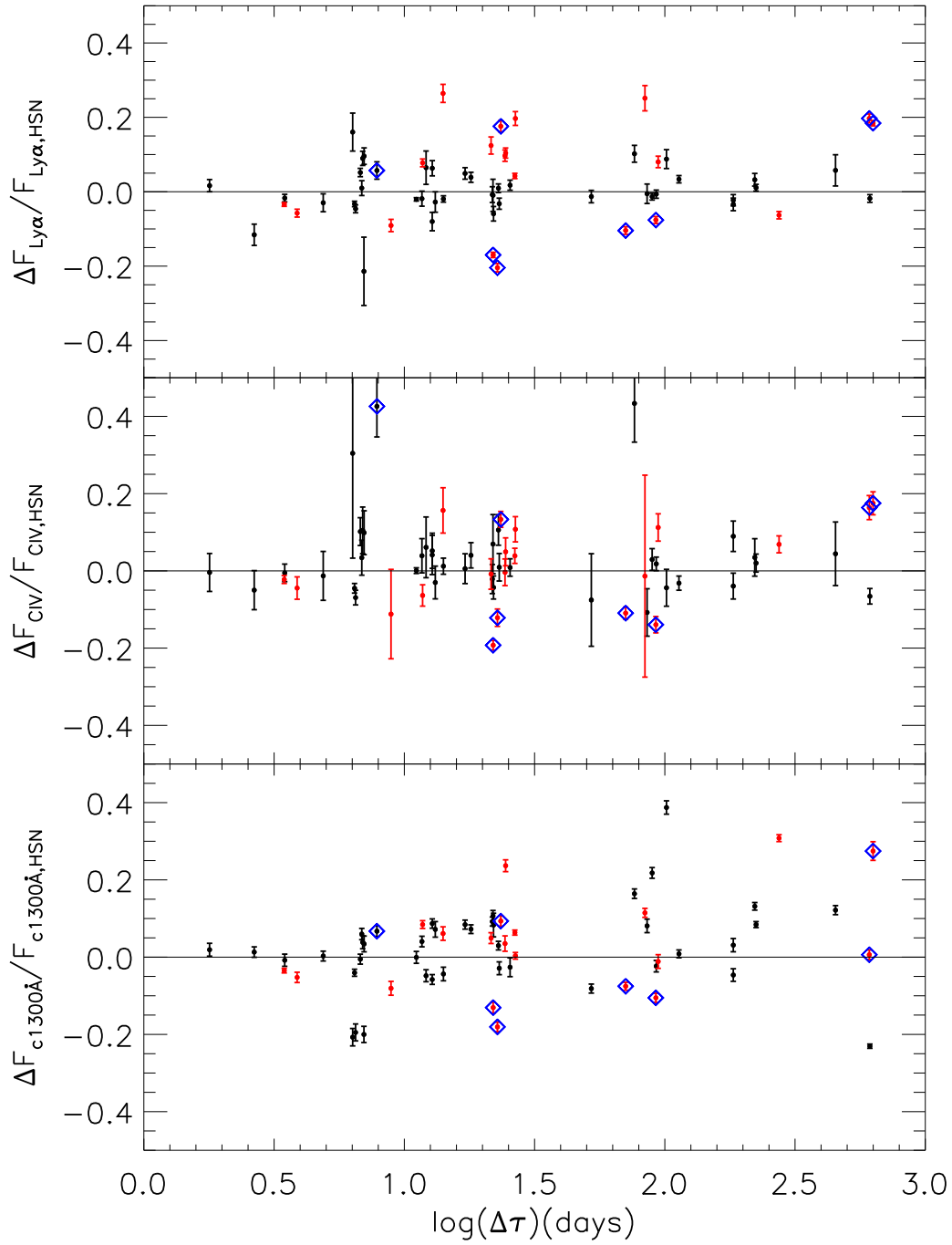


Figure 6. Top: Fractional change in Ly α BEL flux as a function of time between observation epochs in the quasar rest frame on a logarithmic scale, $\log(\Delta\tau)$. Middle: Fractional CIV BEL flux changes vs. $\log(\Delta\tau)$. Bottom: Fractional continuum changes vs. $\log(\Delta\tau)$.

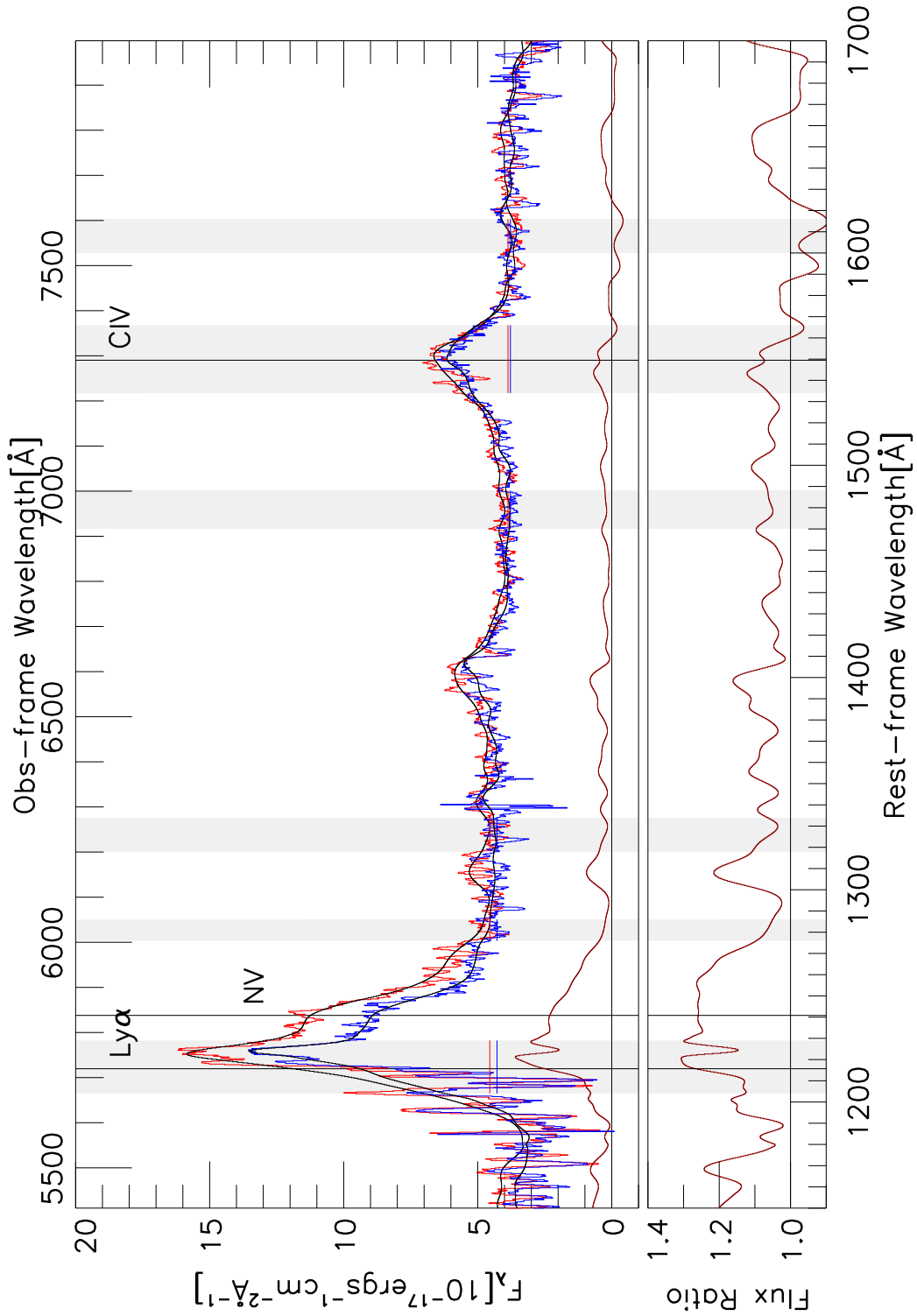


Figure 7. (1) Top: Spectra of SDSS J004240.65+141529.6 at the first HSN-epoch (red) and the second LSN-epoch (blue), and their difference (dark red). Bottom: ratio spectrum.

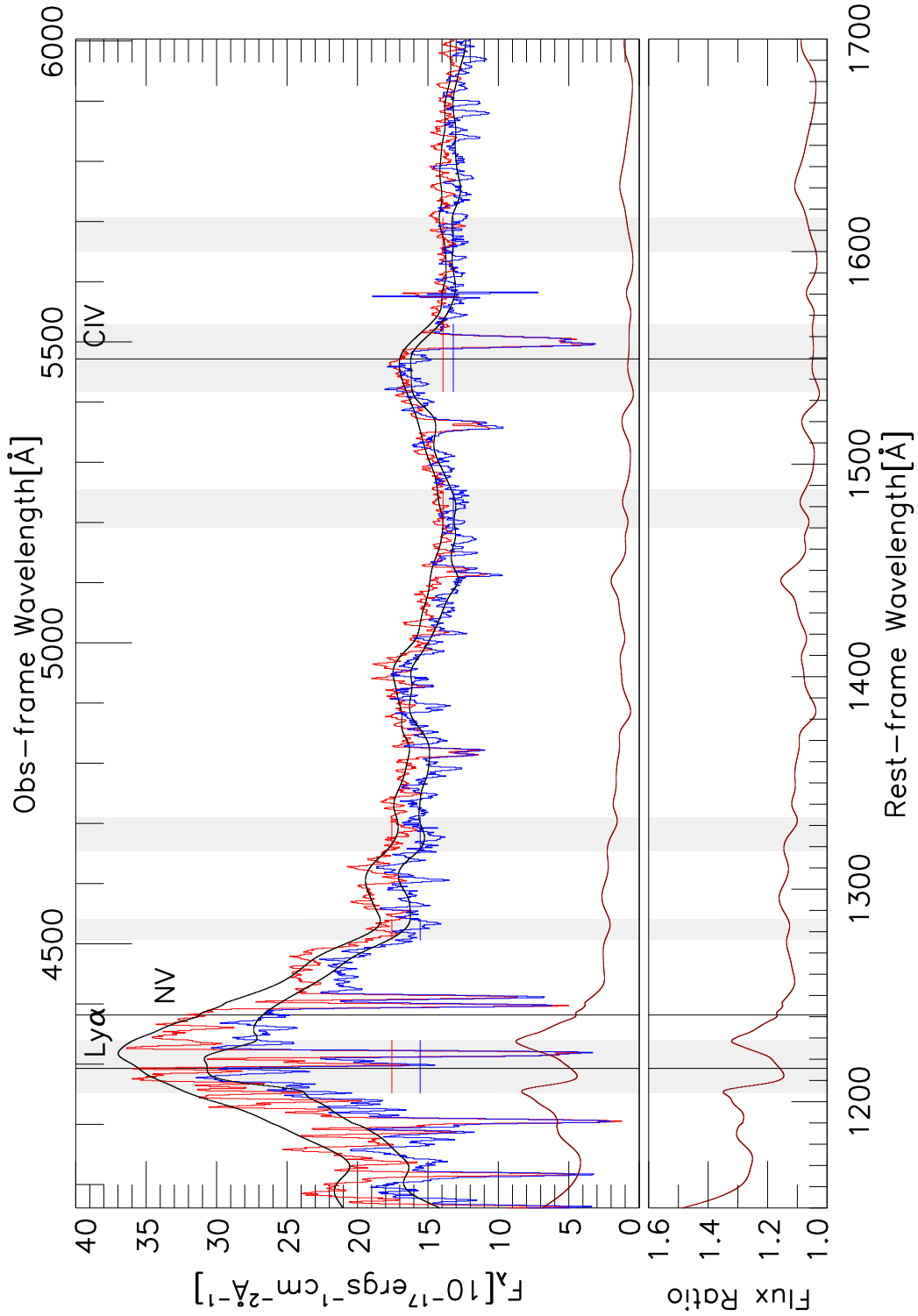


Figure 8. (2) Top: Spectra of SDSS J132750.44+001156.8 at the first LSN-epoch (blue) and the second HSN-epoch (red), and their difference (dark red). Bottom: ratio spectrum.

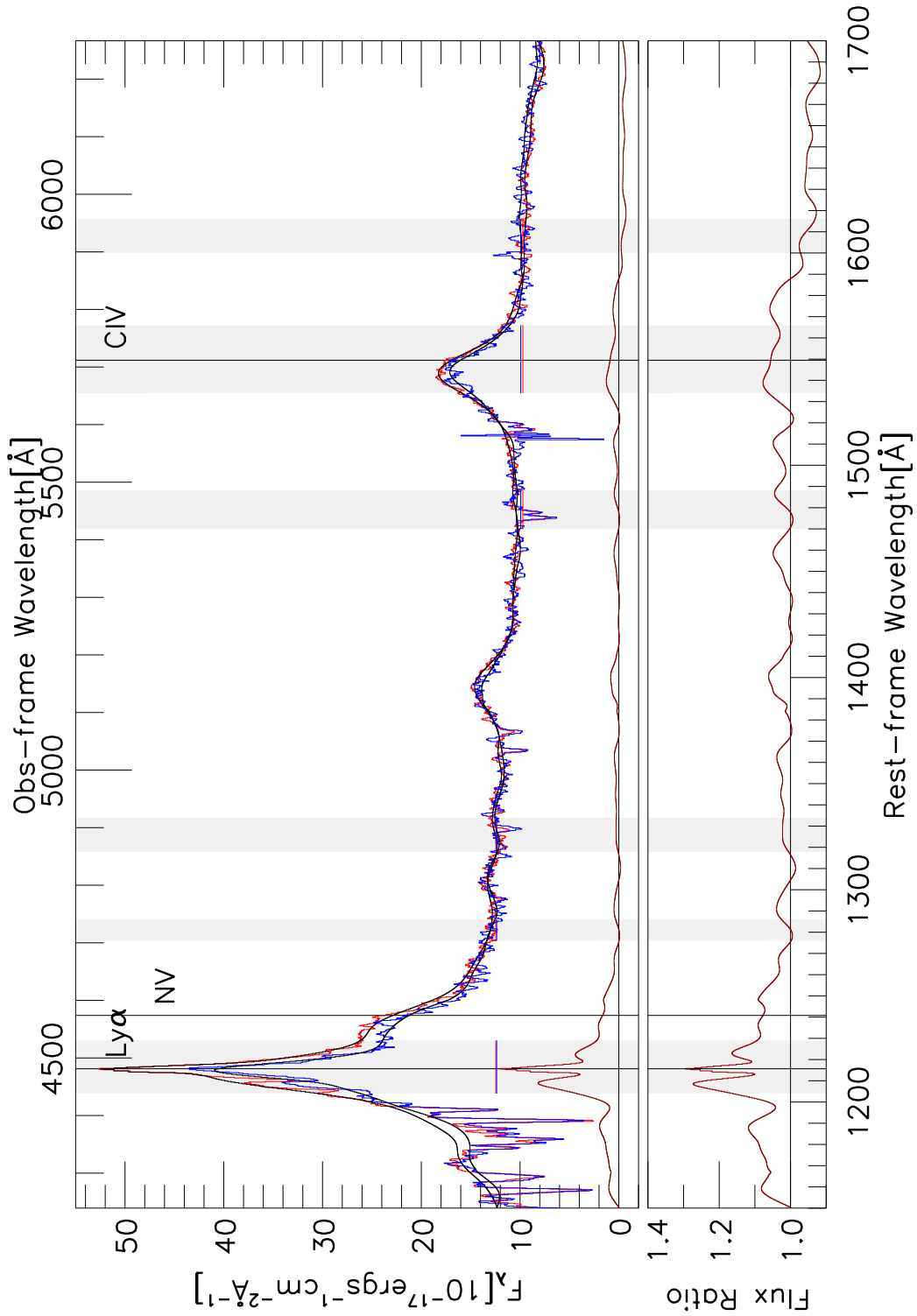


Figure 9. (3) Top: Spectra of SDSS J095106.32+541149.8 at the first LSN-epoch (blue) and the second HSN-epoch (red), and their difference (dark red). Bottom: ratio spectrum.

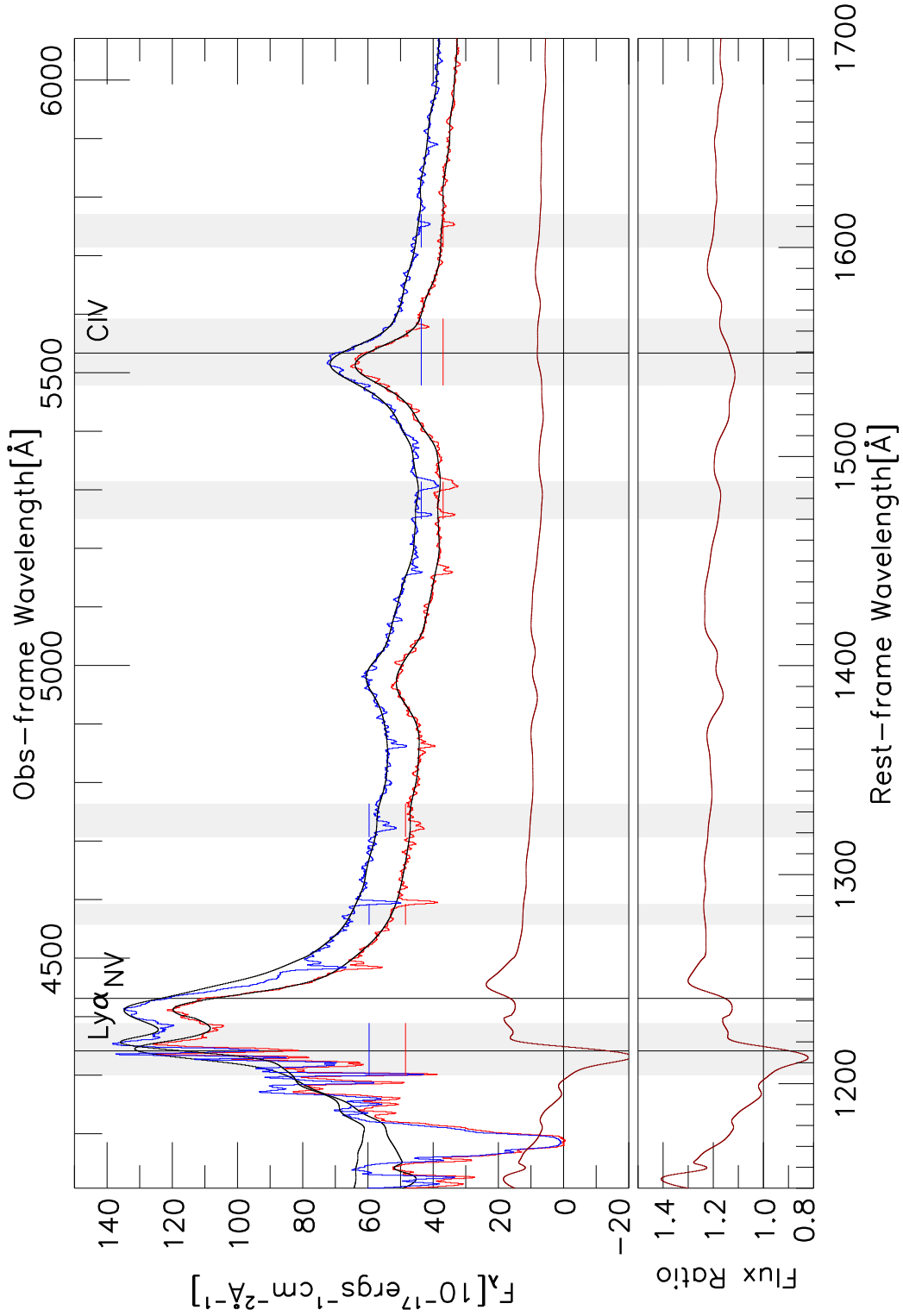


Figure 10. (4) Top: Spectra of SDSS J120802.64+630328.9 at the first HSN-epoch (red) and the second LSN-epoch (blue), and their difference (dark red). Bottom: ratio spectrum.

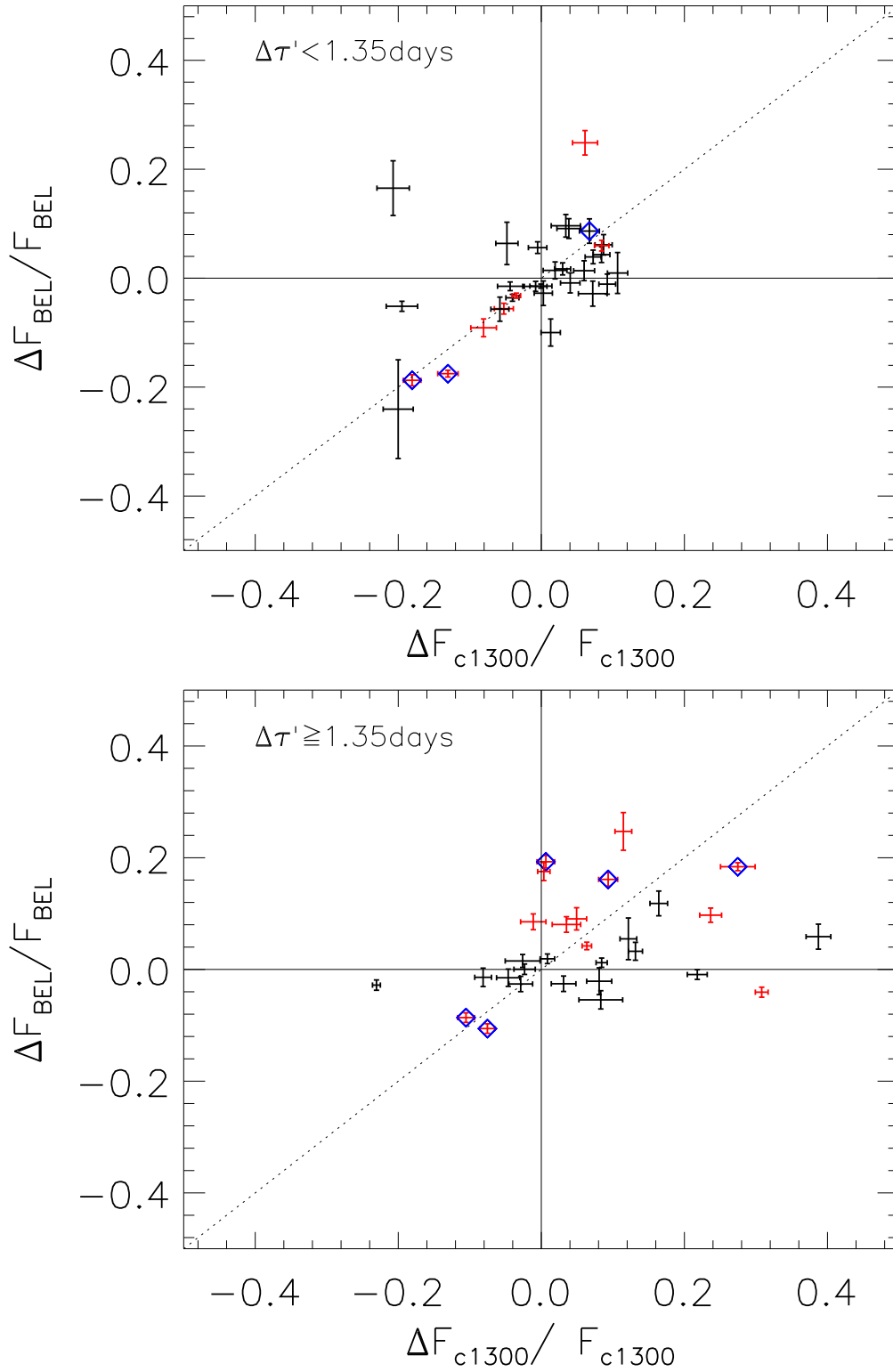


Figure 11. Top: Fractional change in BEL flux vs. fractional change in continuum between two epochs for 32 quasars with $\Delta\tau' < 1.35$ days. Bottom: same as above for 29 quasars with $\Delta\tau' \geq 1.35$ days. See Section 3.5 for the definition of $\Delta\tau'$.

